Asian Journal Science and Engineering

Open Access
Vol. 5, No. 1, June 2026
https://attractivejournal.com/index.php/ajse

Torsional Irregularity Mitigation in Reinforced-Concrete SMRF Buildings Using Hybrid Steel-Braced Eccentrically Braced Frames with RC Beam Links: Effect of Link Length on Seismic Response

Roland Martin Simatupang[1]*, Carrissa Regina Shafi Candraningtyas
[1] *Department of Civil Engineering, Universitas Brawijaya, Malang 65145, East Java, Indonesia*

martin_smtpng@ub.ac.id *

ARTICLE INFO
Article history:
Received
July 15, 2026
Revised
June 17, 2026
Accepted
July 17, 2026

Abstract

Plan torsional irregularity can amplify edge displacement in reinforced-concrete (RC) buildings with asymmetrically distributed lateral stiffness. This numerical study evaluates a hypothetical educational-building model comprising six main stories and a roof level, an RC special moment-resisting frame, and an asymmetrically located RC evacuation-core wall. A hybrid inverted-V eccentric bracing system was introduced on the weaker facade; the diagonal braces were modeled using BJ37 structural-steel H 400 x 400 x 13 x 21 sections, while the intervening RC beam segment acted as the horizontal eccentric link. Four ETABS Ultimate v22.0.0 Build 3628 models were compared by linear-elastic response-spectrum analysis in accordance with SNI 1726:2019: an unbraced baseline and three braced variants with geometric link lengths of 0.50, 1.00, and 1.50 m. Among the three investigated variants, the 0.50 m model produced the lowest combined CM-CR eccentricity and critical edge displacement. In the final signed +/-5% accidental-eccentricity response-spectrum results, the uppermost comparable Joint 25 displacement decreased from 86.33 mm to 22.91 mm in the Y direction (73.5%) and from 65.27 mm to 28.73 mm in the X direction (56.0%). The fundamental period changed from 1.109 s for the baseline to 0.599 s, 0.672 s, and 0.755 s for the 0.50 m, 1.00 m, and 1.50 m variants, respectively. With 15 retained modes, cumulative UX/UY mass participation was 92.88%/95.76% for Model 1, 93.49%/95.26% for Model 2, 93.26%/95.69% for Model 3, and 93.19%/95.50% for Model 4. All four models exceeded 90% cumulative translational mass participation in both principal directions. The signed accidental-eccentricity cases were scaled independently to the applicable equivalent-static minimum base shear before the reported responses were extracted. The bracing system reduced the severity of the source-model torsional indices but did not eliminate torsional irregularity at every story and in both directions. Because the analysis was linear elastic and the link was an RC beam segment rather than a conventional steel EBF link, the results demonstrate comparative global-response trends only and do not establish nonlinear ductility, energy-dissipation capacity, connection adequacy, foundation adequacy, or construction readiness.

Keywords: hybrid eccentric bracing; RC beam link; response-spectrum analysis; SMRF structure; torsional irregularity

Published by	CV. Creative Tugu Pena
ISSN	2963-6752
Website	https://attractivejournal.com/index.php/ajse

INTRODUCTION

Horizontal plan irregularity remains a critical issue in seismic design because a spatial separation between the center of mass (CM) and center of rigidity (CR) couples translational and rotational response. Under a rigid diaphragm, lateral inertia acts through the CM while lateral resistance is mobilized around the CR, producing a torsional moment and unequal edge displacements. SNI 1726:2019 therefore evaluates torsional irregularity from the maximum and average interstory drifts at opposite diaphragm edges under the same signed accidental-eccentricity case [6], [9].

Stiffness asymmetry may arise from nonuniform wall placement, discontinuous framing, or local concentration of lateral-force-resisting elements. Conventional mitigation measures include additional RC walls and concentrically braced frames, but these alternatives can substantially alter force paths and architectural use. Eccentric steel bracing has been investigated as a means of increasing lateral stiffness while retaining an intentional eccentric segment in the beam line [1]-[5]. In deficient RC frames, eccentric steel-brace retrofit has been shown to improve elastic stiffness and strength, although its local connection and link behavior depends strongly on the adopted hybrid detail [1], [2].

The conventional all-steel EBF concept uses a steel link as the designated inelastic fuse. The present study is materially different: BJ37 steel diagonal braces are connected to an RC frame, and the segment of the existing RC beam between brace connection points acts as the horizontal eccentric link. Consequently, steel-link classification and rotation limits cannot be applied directly to the RC segment. The present work is restricted to comparative global elastic response; it does not demonstrate link yielding, cyclic energy dissipation, or connection capacity.

The available literature is dominated by all-steel EBFs and by strength- or drift-oriented retrofit studies. Comparatively limited evidence is available on the global torsional response of asymmetric RC frames strengthened by steel eccentric braces when the existing RC beam acts as the horizontal link, particularly for controlled variation of link geometry [1]-[5]. To address this narrower gap, a hypothetical building model was developed from preliminary design, with an asymmetrically placed RC evacuation-core wall intentionally creating the baseline stiffness imbalance.

The objectives of this study are:

(1) To quantify CM-CR eccentricity and storywise global torsional-response indices in the baseline and strengthened models.

(2) To compare absolute edge displacement and amplified design-story drift under design response-spectrum loading.

(3) To quantify member-level axial force, shear, flexural moment, and torsional-moment redistribution in selected beams and columns after brace installation, while evaluating global diaphragm torsion separately.

Section 2 presents the governing torsional-response and hybrid EBF concepts. Section 3 describes the case-study geometry, material properties, numerical assumptions, accidental-torsion procedure, and response-spectrum analysis. Section 4 reports the modal, base-shear, eccentricity, displacement, drift, torsional-response, and internal-force results. Section 5 summarizes the findings, limitations, and requirements for further nonlinear, connection-level, and foundation research.

2. THEORETICAL BACKGROUND

A. Torsional Irregularity and CM-CR Eccentricity

For each rigid diaphragm i, the inherent plan eccentricity is calculated from the coordinates of the CM and CR. The relevant coordinate difference is measured perpendicular to the direction of seismic action. A large inherent eccentricity is an indicator of stiffness imbalance, but the SNI torsional-irregularity classification is based on the ratio of edge interstory drifts rather than eccentricity alone [9].

$$e_{0,i} = |CM_i - CR_i| \quad (1)$$

The maximum interstory drift at either extreme edge, Delta_max,i, is compared with the mean of the two edge drifts, Delta_avg,i. Ratios above 1.2 and 1.4 indicate Type A and Type B torsional irregularity, respectively. The ratio must be determined from the same load case and seismic direction, including accidental torsion.

$$eta_i = Delta_{max,i} / Delta_{avg,i} \quad (2)$$

Accidental torsion represents uncertainty in mass and stiffness distribution by shifting the diaphragm mass center by 5% of the plan dimension perpendicular to the applied force. Where amplification is required, SNI 1726:2019 defines the torsional amplification factor as follows [9].

$$Ax_i = [Delta_{max,i} / (1.2\ Delta_{avg,i})]^2, \quad 1.0 <= Ax_{,i} <= 3.0 \quad (3)$$

$$ea_{,i} = 0.05\ b_{perp}\ Ax_{,i} \quad (4)$$

The factor Ax amplifies the accidental-eccentricity component and is evaluated story by story. Signed positive and negative accidental-eccentricity cases are required because the governing edge response may reverse with the sign of the offset.

B. Conventional Steel EBF Behavior and the Present Hybrid System

In a conventional steel EBF, brace forces are transferred through an intentionally short beam segment that is proportioned to yield before the surrounding brace, beam, and column members. Steel-link behavior is commonly described using the normalized length e/(Mp/Vp), with shorter links tending toward shear-dominated response and longer links toward flexural response [4], [8]. These rules are relevant background for all-steel EBF mechanics but are not adopted as acceptance criteria for the RC beam segment in this study.

Because the eccentric segment is reinforced concrete, the tested values of 0.50, 1.00, and 1.50 m are treated as geometric link-length variants used to compare elastic global stiffness and torsional response. RC link strength, cracking, confinement, anchorage, chord rotation, and cyclic degradation require separate evaluation under RC provisions such as SNI 2847:2019 and through experimental or validated nonlinear modeling [10]. Shayanfar [3] is cited only to illustrate the sensitivity of EBF response to link configuration; that work used a vertical steel link and does not directly validate the horizontal RC link considered here.

C. Scope of the Global Linear Evaluation

Linear response-spectrum analysis combines modal maxima and is appropriate for comparative elastic demand assessment when code scaling and directional combination rules are satisfied [6], [9], [16]. It cannot activate concentrated plastic hinges or reproduce yielding sequence, brace buckling, cyclic degradation, residual drift, or energy dissipation. Accordingly, this study interprets shorter computed period, lower edge displacement, reduced CM-CR eccentricity, and changed member forces as global elastic-response trends only.

3. METHODOLOGY

A. Case-Study Building and Geometry

The numerical case study is a hypothetical reinforced-concrete educational-building model located in Malang, East Java, for seismic-input purposes. It contains six main stories and a roof level. The first story is 4.725 m high, Stories 2-6 are 4.0 m high, and the roof level is 2.1 m high, giving a total height of 26.825 m. The plan dimensions are 32.4 m x 28.8 m, corresponding to approximately 933.12 m2 per main floor. A 250 mm RC wall surrounds an asymmetrically positioned evacuation core and intentionally creates the baseline stiffness imbalance. Complete preliminary-design calculations, member schedules, and drawings are intended for supplementary material.

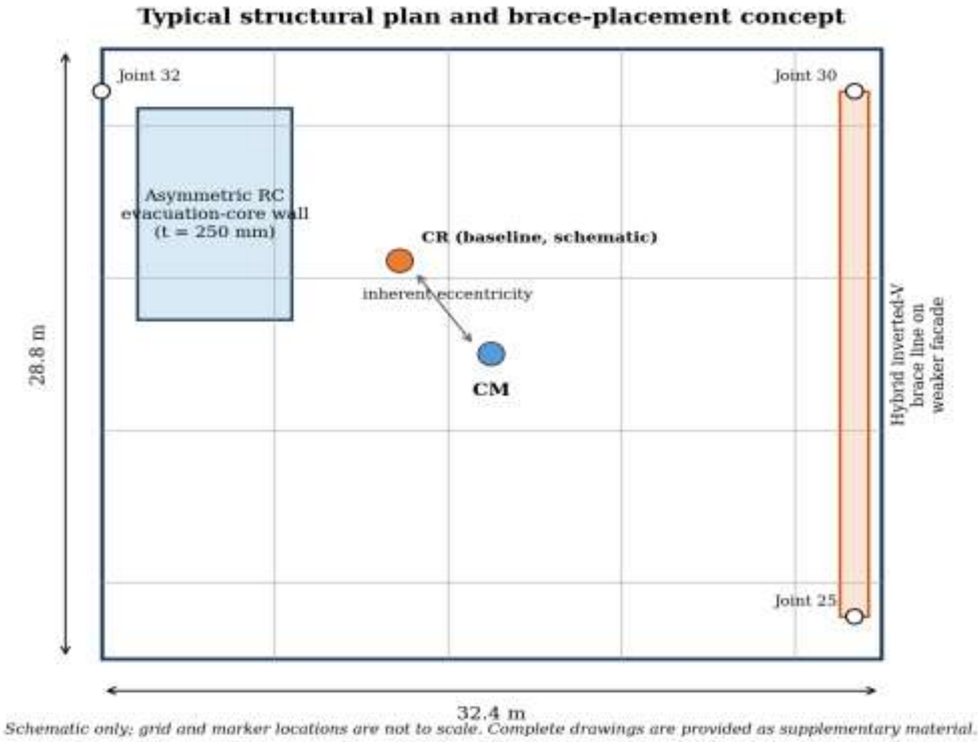

Figure 1. Schematic typical plan, asymmetric RC core, braced facade, and representative extreme joints used for torsional-response evaluation.

Table 1. Summary of structural geometry used in the numerical model

Model parameter	Adopted value
Building type	Hypothetical RC educational-building model
Modeled levels	Six main stories plus roof level (seven levels total)
Plan dimensions	32.4 m x 28.8 m
Approximate floor area	933.12 m2 per main floor
Story heights	Level 1: 4.725 m; Levels 2-6: 4.0 m; roof: 2.1 m
Total height	26.825 m to roof peak
Primary beams	B1 350x600; B4 300x500; B6 250x500; B7 250x400; B8 250x350; B9 200x350 mm
Secondary beams	B5 350x450; B6a 250x500; B7a 250x400; B9a 200x350; B10a 200x300 mm
Columns	600x600 mm and 500x500 mm
Slab	120 mm RC slab; rigid diaphragm
Shear wall	250 mm RC wall at asymmetric evacuation core
Boundary condition	Fixed bases; soil-structure interaction excluded

B. Materials and Hybrid Brace-Link Configuration

Concrete compressive strengths of f'c = 33.2 MPa and 24.9 MPa were used for columns/walls and beams/slabs, respectively. The diagonal brace members were modeled using BJ37 structural steel with fy = 240 MPa, fu = 370 MPa, and E = 200 GPa. This 240 MPa value applies to the structural-steel brace profile and not to the RC longitudinal reinforcement. The final RC reinforcing-steel grade must be confirmed from the ETABS material definition and reinforcement schedule; the preliminary-design calculations use deformed reinforcement with fy = 420 MPa.

Table 2. Material and hybrid brace-link modeling properties

Component	Property / modeling assumption
Columns and RC walls	f'c = 33.2 MPa
RC beams and slabs	f'c = 24.9 MPa
RC reinforcing steel	Deformed bars; fy = 420 MPa in preliminary design
Brace structural steel	BJ37; fy = 240 MPa; fu = 370 MPa; E = 200 GPa
Brace section	H 400x400x13x21; A = 218.69 cm2; Ix = 201000 cm4; Iy = 10800 cm4
Brace-end idealization	Moment releases at both ends; predominantly axial response
Horizontal link	Segment of the RC beam between brace connection points
Brace-to-RC connection	Coincident global-model joints; local gusset/anchor behavior excluded

The steel braces are arranged as inverted-V elements on the external facade opposite the asymmetric core, where the baseline model exhibited lower lateral stiffness and larger deformation. The RC beam segment between the brace connection points forms the horizontal eccentric link. Brace ends are moment-released so that the brace members primarily transfer axial force. Connection nodes are idealized as coincident; gusset plates, anchors, local RC bearing, confinement, and force transfer are not explicitly modeled.

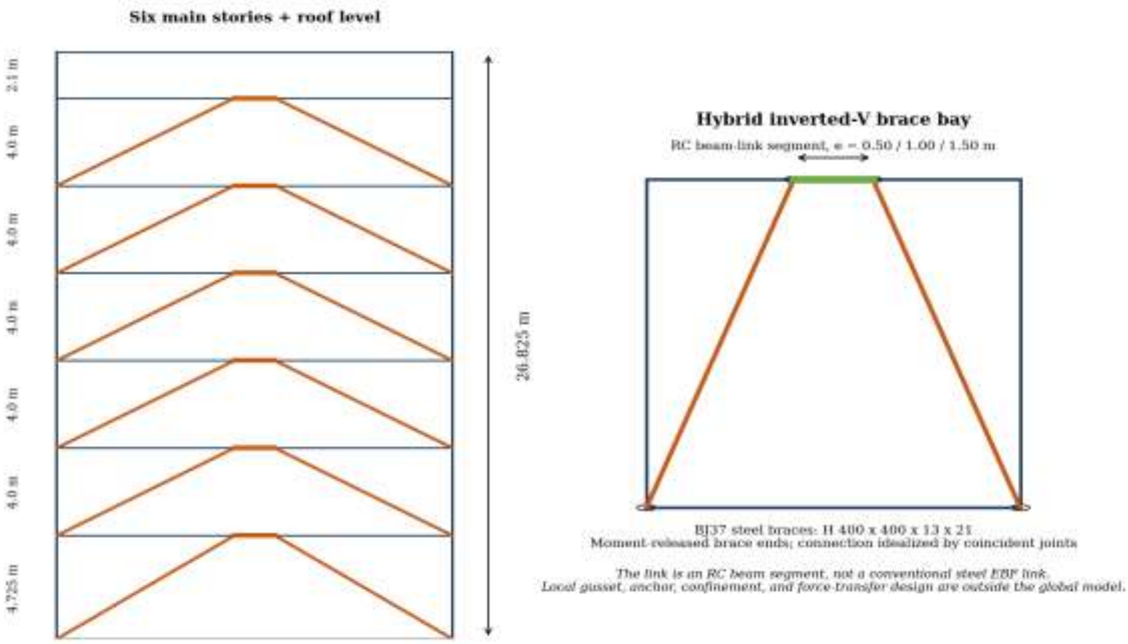

Figure 2. Building-height scheme and hybrid inverted-V steel-brace / RC beam-link idealization.

C. Structural Model Variants

Table 3. Controlled model variants

Model	Description
Model 1	Baseline RC frame and asymmetric RC core; no added braces
Model 2	Hybrid inverted-V braces with geometric RC link length e = 0.50 m
Model 3	Hybrid inverted-V braces with geometric RC link length e = 1.00 m
Model 4	Hybrid inverted-V braces with geometric RC link length e = 1.50 m

All four models retain the same building geometry, material definitions, gravity loads, diaphragm assumptions, and seismic input. Only the presence of the brace system and the geometric distance between the brace connection points are varied. The term “best-performing” is used only for the variant producing the lowest combined elastic-response measures among these three tested link lengths; no mathematical or nonlinear optimization is claimed.

D. Numerical Model and Seismic Analysis

The updated numerical analyses were performed in ETABS Ultimate v22.0.0 Build 3628 [16]. RC beams and columns were represented by frame elements, walls and slabs by shell elements, and floor slabs were assigned as rigid diaphragms. Fixed supports were assigned at the base. Cracked-section stiffness modifiers followed the source model: 0.70Ig for columns and walls, 0.35Ig for beams, and 0.25Ig for slabs. Beam torsional stiffness was reduced to 0.001 of the gross value to avoid unrealistically high torsional restraint. Gravity loads were assigned in accordance with SNI 1727:2020 [11].

The site was classified as Site Class SD. The source model used Ss = 0.87, S1 = 0.41, SDS = 0.668, and SD1 = 0.513, with Risk Category IV, Ie = 1.5, R = 7, Cd = 5.5, and Omega0 = 2.5. Modal responses were combined using the complete quadratic combination (CQC) method, and orthogonal directional effects were included through the adopted 100%/30% combination [6], [9], [16]. Fifteen eigenmodes were extracted for each final model. The cumulative translational participating-mass ratios reached at least 90% in both principal horizontal directions for all four models. Each response-spectrum result was scaled to the applicable equivalent-static minimum base shear. This global base-shear scaling was applied independently from the signed +/-5% accidental-eccentricity offsets.

All reported response quantities were obtained from linear-elastic RSA. No nonlinear hinge response was activated or interpreted. Any hinge definitions retained in preliminary model files do not contribute to a linear response-spectrum case and are outside the present study.

E. Accidental Torsion and Drift Evaluation

Separate unshifted and signed accidental-eccentricity response-spectrum cases were defined as RSX, RSX(+), RSX(-), RSY, RSY(+), and RSY(-). A diaphragm mass-center offset equal to 5% of the plan dimension perpendicular to the excitation direction was explicitly assigned in ETABS for each positive and negative case. The governing response was selected from the signed cases. All reported displacement, drift, torsional-response, and internal-force results were extracted from these final +/-5% accidental-eccentricity cases after response-spectrum base-shear scaling. The response-spectrum base-shear scale factor and the storywise torsional amplification factor Ax are distinct quantities. The final numerical models include the prescribed signed 5% accidental eccentricity; no additional storywise Ax-based enlargement beyond the explicitly modeled 5% offset is claimed.

Absolute joint displacement is distinguished from interstory drift. For the drift evaluation, elastic story drift delta_e was calculated from the difference between adjacent-level Joint 25 displacements obtained from the governing final signed +/-5% accidental-eccentricity cases. The design drift was amplified as Delta = (Cd/Ie)delta_e. For the adopted Risk Category IV model under the “all other structures” category, the allowable drift was taken as Delta_a = 0.010hsx [9]. The resulting tables provide a code-oriented screening at the evaluated edge line; they do not replace verification of every required edge line and governing load combination.

$$\mathrm{Delta}_i = (Cd / Ie)\ \mathrm{delta}_{e,i} \tag{5}$$

F. Evaluation Parameters and Model Verification

Table 4. Numerical-model verification and validation scope

Check	Procedure	Status
Preliminary member sizing	Beam, column, slab, and wall dimensions checked by hand under SNI 2847:2019	Completed in source report
CM and CR	Software coordinates independently checked for selected levels	Completed; selected values in supplement
Period bound	Computed T1 checked against Ta and CuTa; modal tables and available solver logs reviewed	M1: 1.109 s; M2: 0.599 s; M3: 0.672323 s; M4: 0.754948 s. M3/M4 logs: 15 modes and zero negative stiffness eigenvalues
Modal participation	Cumulative translational participation required to reach at least 90% in X and Y	Mode 15 SumUX/SumUY: M1 0.9288/0.9576; M2 0.9349/0.9526; M3 0.9326/0.9569; M4 0.9319/0.9550.
Base-shear scaling	RSA base shear scaled to equivalent-static minimum	Reported in Table 6
External benchmark	Experimental or validated hybrid-link benchmark	Not performed; limitation

The comparison uses: (i) computed and code-limited periods; (ii) response-spectrum base-shear scaling; (iii) CM-CR eccentricity; (iv) critical edge displacement and amplified story drift; (v) storywise torsional ratio eta; and (vi) axial, shear, flexural, and torsional demands in selected elements. Internal-force envelopes were extracted from the same load-combination set for Models 1 and 2. The ETABS modal participating-mass tables for all four models contain 15 modes. At Mode 15, the cumulative UX/UY ratios are 0.9288/0.9576 for Model 1, 0.9349/0.9526 for Model 2, 0.9326/0.9569 for Model 3, and 0.9319/0.9550 for Model 4. Thus, all four final models exceed 90% cumulative translational mass participation in both principal directions.

4. RESULTS AND DISCUSSION

A. Modal Properties and Base-Shear Scaling

Table 5. Comparative fundamental periods and translational modal-mass participation

Model	Link (m)	T1 (s)	Mode at 90% X	Mode at 90% Y	Sum UX at 15	Sum UY at 15
Model 1	-	1.109	12	15	0.9288	0.9576
Model 2	0.50	0.599	11	14	0.9349	0.9526
Model 3	1.00	0.672	11	14	0.9326	0.9569
Model 4	1.50	0.755	12	15	0.9319	0.9550

The modal results show a clear change in both period and modal character after bracing. Model 1 has T1 = 1.109 s; its first mode is strongly coupled in Y translation and torsion (UY = 0.3351; RZ = 0.3469), while the largest first-cycle X contribution occurs in Mode 2 (UX = 0.5849). Model 2 has T1 = 0.599 s and a predominantly X-translational first mode (UX = 0.5077); its largest torsional contribution occurs in Mode 3 (RZ = 0.4830) together with UY = 0.2575. Model 3 has T1 = 0.672 s, with coupled first-mode participation (UX = 0.3311; UY = 0.2570; RZ = 0.2225), and Model 4 has T1 = 0.755 s, with UX = 0.2405, UY = 0.2985, and RZ = 0.2852 in Mode 1. Relative to the unbraced model, T1 is reduced by approximately 46.0%, 39.4%, and 31.9% for Models 2, 3, and 4, respectively. The monotonic increase in T1 from the 0.50 m to the 1.50 m link variant indicates a progressive reduction in global elastic stiffness as the geometric link length increases. The cumulative-mass criterion is satisfied by Model 2 at Modes 11 (X) and 14 (Y), by Model 3 at Modes 11 (X) and 14 (Y), and by Model 4 at Modes 12 (X) and 15 (Y). Model 1 reaches the X threshold at Mode 12 and Y at Mode 15. The Model 3 and Model 4 solver logs confirm 15 extracted modes, zero negative stiffness eigenvalues, and use of the complete modal set in all signed RSA cases.

Table 6. Equivalent-static minimum and unscaled RSA base-shear values

Model	Vstatic min. (kN)	Vt,X (kN)	Vt,Y (kN)	Scale X	Scale Y
Model 1	8997.1	5664.5	4493.6	1.588	2.002
Model 2	9063.3	5744.9	4945.6	1.578	1.833
Model 3	9061.0	5266.1	4560.2	1.721	1.987
Model 4	8815.2	5201.4	4456.5	1.695	1.978

The unscaled dynamic base shears and required scaling factors vary with both period and modal response. Model 2 has a slightly higher equivalent-static minimum than Model 1 because of the changed model mass and period treatment, while Models 3 and 4 require larger X-direction scale factors than Model 2. These results demonstrate why brace effects should be interpreted from the complete scaled response rather than from stiffness alone.

B. CM-CR Eccentricity

Table 7. Average total CM-CR eccentricity from the source models

Model	eX (m)	eY (m)	Reduction X (%)	Reduction Y (%)
Model 1	15.220	7.259	-	-
Model 2	11.120	5.860	26.94	19.28
Model 3	12.870	6.320	15.44	12.94
Model 4	13.400	6.740	11.96	7.15

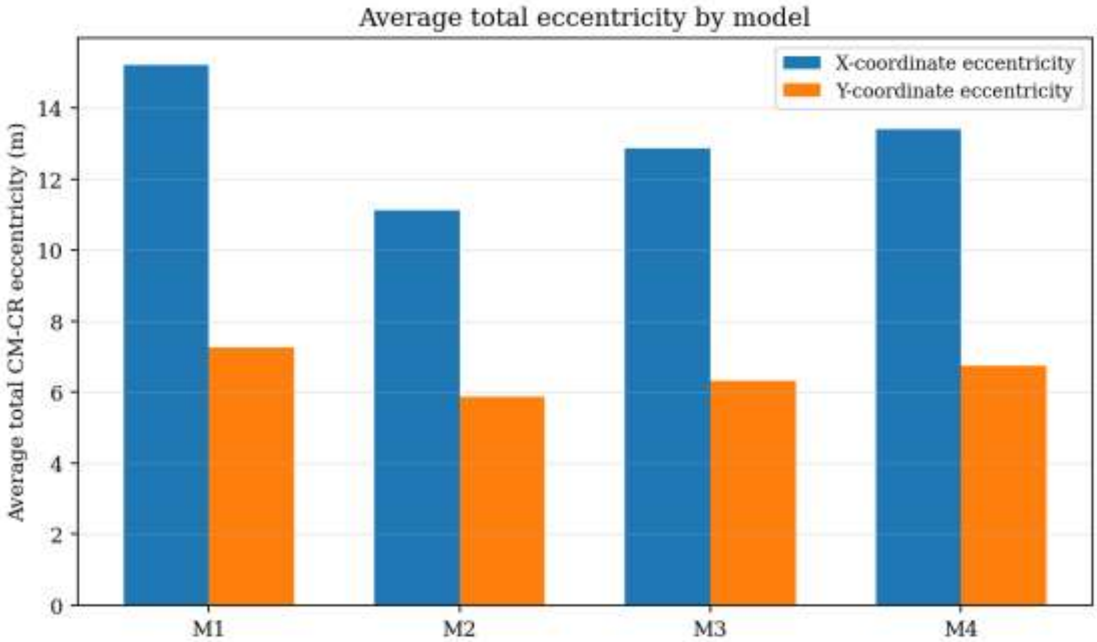

Figure 3. Average total CM-CR eccentricity in the four source models.

Among the three braced variants, Model 2 achieved the lowest average total eccentricity in both coordinate directions. Relative to Model 1, its average X- and Y-coordinate eccentricities decreased by approximately 26.9% and 19.3%, respectively. Models 3 and 4 also reduced eccentricity, but the effect diminished as the geometric link length increased. The result supports selection of Model 2 as the best-performing tested variant for the combined global elastic metrics, although it does not by itself establish torsional regularity.

C. Critical Edge Displacement and Story-Drift Screening

Table 8. Uppermost comparable main-story Joint 25 displacement

Model	UY (mm)	Y reduction (%)	UX (mm)	X reduction (%)
Model 1	86.33	-	65.27	-
Model 2	22.91	73.5	28.73	56.0
Model 3	35.20	59.2	33.18	49.2
Model 4	47.80	44.6	41.37	36.6

The model contains six main stories and a roof level. The comparable extreme-joint series terminates at Story 6 because the roof level has a different plan and no geometrically consistent pair of edge joints. These are absolute joint displacements, not interstory drifts.

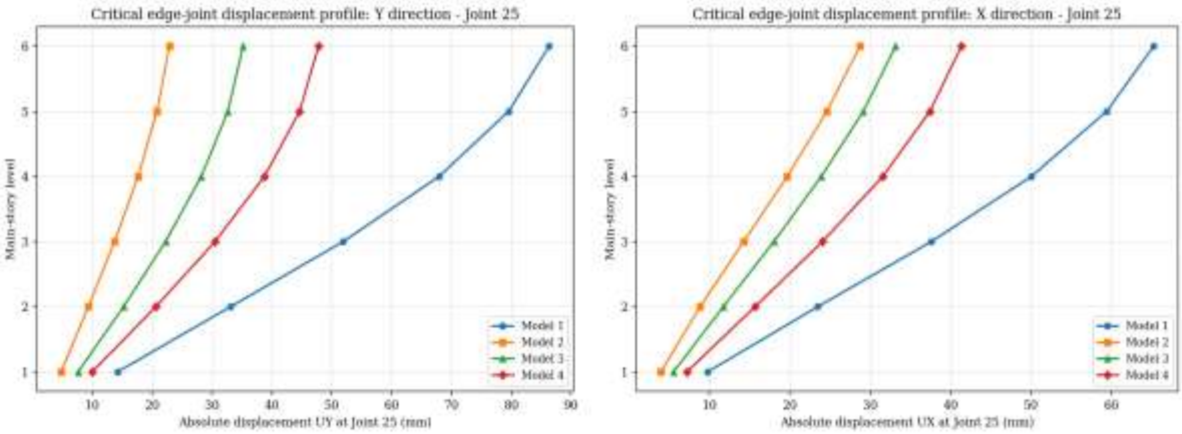

Figure 4. Critical edge-joint displacement profiles at Joint 25: (a) Y direction and (b) X direction.

At Story 6, Model 2 reduced the critical Joint 25 displacement from 86.33 mm to 22.91 mm in the Y direction (73.5%) and from 65.27 mm to 28.73 mm in the X direction (56.0%). Models 3 and 4 showed smaller reductions, consistent with their longer periods and higher global flexibility. The former manuscript values of 23.21 mm and 7.08 mm were transcription errors and have been removed.

Table 9. Amplified design-drift screening - X direction

Story	Delta_a (mm)	M1: Delta (U, P/F)	M2: Delta (U, P/F)	M3: Delta (U, P/F)	M4: Delta (U, P/F)
1	47.2	35.9 (0.76, P)	14.6 (0.31, P)	20.3 (0.43, P)	26.5 (0.56, P)
2	40.0	50.2 (1.26, F)	17.9 (0.45, P)	22.8 (0.57, P)	31.1 (0.78, P)
3	40.0	51.8 (1.29, F)	19.9 (0.50, P)	23.1 (0.58, P)	30.8 (0.77, P)
4	40.0	45.7 (1.14, F)	19.8 (0.50, P)	21.6 (0.54, P)	27.5 (0.69, P)
5	40.0	34.4 (0.86, P)	18.1 (0.45, P)	19.2 (0.48, P)	21.5 (0.54, P)
6	40.0	21.4 (0.53, P)	15.1 (0.38, P)	14.7 (0.37, P)	14.4 (0.36, P)

Delta = (Cd/Ie) delta_e with Cd/Ie = 5.5/1.5; Delta_a = 0.010hsx for the adopted Risk Category IV screening. U = utilization; P/F = screening pass/fail.

Table 10. Amplified design-drift screening - Y direction

Story	Delta_a (mm)	M1: Delta (U, P/F)	M2: Delta (U, P/F)	M3: Delta (U, P/F)	M4: Delta (U, P/F)
1	47.2	52.2 (1.11, F)	17.6 (0.37, P)	28.1 (0.59, P)	36.6 (0.77, P)
2	40.0	69.3 (1.73, F)	16.7 (0.42, P)	27.8 (0.69, P)	39.1 (0.98, P)
3	40.0	68.9 (1.72, F)	16.1 (0.40, P)	25.7 (0.64, P)	36.2 (0.91, P)
4	40.0	58.8 (1.47, F)	14.4 (0.36, P)	21.9 (0.55, P)	30.3 (0.76, P)
5	40.0	42.6 (1.07, F)	11.6 (0.29, P)	16.3 (0.41, P)	21.6 (0.54, P)
6	40.0	24.8 (0.62, P)	7.7 (0.19, P)	9.3 (0.23, P)	11.5 (0.29, P)

Delta = (Cd/Ie) delta_e with Cd/Ie = 5.5/1.5; Delta_a = 0.010hsx for the adopted Risk Category IV screening. U = utilization; P/F = screening pass/fail.

The screening indicates that the baseline critical-edge drift exceeds the adopted allowable value in both directions, whereas the three braced variants remain below the limit at the evaluated Joint 25 line. Model 4 approaches the Y-direction limit at the lower stories. These outcomes are based on the final signed +/-5% accidental-eccentricity and base-shear-scaled RSA cases. They should be interpreted as a line-specific screening rather than a complete code-compliance statement because all required edge lines and governing load combinations must be checked.

D. Torsional-Irregularity Screening

Table 11. Storywise torsional-ratio ranges from the final signed accidental-eccentricity results

Model	Direction	eta range	Stories: none / Type A / Type B
Model 1	X	1.05-1.45	1/2/3
Model 1	Y	1.60-1.83	0/0/6
Model 2	X	1.09-1.31	2/4/0
Model 2	Y	1.22-1.65	0/2/4
Model 3	X	1.02-1.36	3/3/0
Model 3	Y	1.24-1.74	0/1/5
Model 4	X	1.03-1.40	2/3/1
Model 4	Y	1.34-1.79	0/1/5

Model 2 reduced the X-direction range from 1.05-1.45 to 1.09-1.31 and the Y-direction range from 1.60-1.83 to 1.22-1.65. In the source classifications, the X direction contains either no irregularity or Type A response, while Type B response remains at several lower stories in the Y direction. Model 3 yields slightly lower X-direction torsional ratios at several upper stories, but Model 2 performs better in the critical Y direction and produces lower eccentricity and displacement overall. Model 4 generally shows the largest remaining torsional ratios among the braced variants.

These results support the conclusion that the brace system mitigates torsional severity but does not render the building torsionally regular at every level. The applicable amplification, analysis, and detailing requirements therefore remain necessary. No blanket direction-wide "Type B to Type A" reclassification is made.

E. Internal-Force Redistribution

Table 12. Representative axial-force and shear-demand redistribution from Model 1 to Model 2

Element	Location	Action	Model 1	Model 2	Change
C65	Non-braced column	P (kN)	1762.18	1606.23	-8.85%
C44	Non-braced column	P (kN)	3466.37	3412.64	-1.55%
C59	Braced-zone column	P (kN)	1881.69	-662.69	Envelope sign reversal
C64	Braced-zone column	P (kN)	2305.19	-1833.72	Envelope sign reversal
B31	Braced-zone beam	V2 (kN)	254.39	911.75	+258%
B37	Braced-zone beam	V2 (kN)	197.21	1545.79	+684%
B83	Braced-zone beam	V2 (kN)	157.94	1537.01	+873%
B111	Braced-zone beam	V2 (kN)	272.84	1312.35	+381%
C59	Braced-zone column	V2 (kN)	125.76	45.97	-63.4%
C64	Braced-zone column	V2 (kN)	102.07	45.85	-55.1%

The braces create a new axial-force path and concentrate beam shear in the braced bays. Representative braced beams show shear-demand increases of approximately 258%-873%, substantially larger than the 136% value quoted in the former condensed draft. In contrast, selected columns show lower shear demand after brace installation. The axial-force envelope of C59 and C64 changes sign, demonstrating a substantial redistribution of member demand. The physical interpretation of tension or compression must follow the final ETABS sign convention and governing load combination.

Table 13. Representative member torsion and flexural-moment envelopes

Element	Location	T M1 (kNm)	T M2 (kNm)	M3 M1 (kNm)	M3 M2 (kNm)
B31	Braced beam	6.42	0.83	-231.16	-191.53
B37	Braced beam	6.12	2.04	-340.93	-323.44
B83	Braced beam	6.28	2.24	-262.74	-307.27
B111	Braced beam	5.82	1.39	-306.74	-299.25
C59	Braced column	45.14	11.71	336.59	96.19
C64	Braced column	45.14	11.71	142.08	-39.79

Torsional demand decreases in the selected braced-zone elements, whereas flexural-moment changes are not uniformly monotonic. The table reports demand redistribution, not member capacity.

The selected braced-zone beams and columns exhibit markedly lower member torsion in Model 2, but flexural moments do not decrease uniformly: for example, the magnitude of B83 M3 increases. It is therefore inappropriate to summarize the response as a universal 15%-40% moment reduction. The correct interpretation is that the added brace system changes the distribution and sign of axial, shear, flexural, and torsional demands across the frame.

The reported RC link-region shear is an elastic demand from the global model, not a demonstrated RC link capacity. Construction application requires a separate SNI 2847 strength and detailing check, including shear capacity, confinement, anchorage, brace-gusset force transfer, and capacity protection of adjacent members. Similarly, because the numerical model assumes fixed bases, the observed axial-force redistribution cannot be interpreted as proof of foundation adequacy. Governing support reactions must be checked for compression, uplift, overturning, sliding, and soil or pile capacity before implementation.

F. Limitations, Constructability, and Further Research

The principal limitation is the linear-elastic analysis scope. The numerical response does not establish RC link yielding, chord-rotation capacity, brace buckling, cyclic degradation, residual drift, or energy dissipation. The brace-to-RC connection is idealized by coincident nodes, and local gusset, anchor, concrete bearing, splitting, confinement, and bar-anchorage mechanisms are excluded. The fixed-base model excludes soil-structure interaction and foundation flexibility, which may affect periods, torsional response, and support demand.

No cost estimate, construction sequence, fire or corrosion-protection study, or operational-disruption assessment was performed. External facade placement may reduce interior interference, but project-specific constructability must address access, temporary shoring, gusset and anchor installation, RC beam local strengthening, architectural conflicts, fireproofing, corrosion protection, and possible foundation strengthening. Accordingly, the system is not described as cost-effective or construction-ready.

Future work should include nonlinear static analysis and incremental dynamic analysis (IDA). For IDA, ground-motion records should be incrementally scaled using 5%-damped Sa(T1) or an averaged spectral acceleration around T1, from elastic response to dynamic instability, while monitoring maximum and residual story drift, diaphragm rotation, RC link chord rotation, brace axial demand, connection force transfer, and support reactions. Quasi-static cyclic testing of representative RC link and steel-to-RC connection assemblies should quantify cracking and yielding sequence, shear strength, chord rotation at first yield and peak strength, rotation at 20% post-peak strength loss, stiffness and strength degradation, cumulative energy dissipation, anchorage behavior, and failure mode.

5. CONCLUSION

This study compared the linear-elastic seismic response of a hypothetical RC SMRF building before and after the addition of hybrid inverted-V steel braces connected through RC beam-link segments. The following conclusions are drawn from the final numerical-model results:

(1) Within the three tested geometric link lengths, the 0.50 m variant produced the largest combined reduction in average CM-CR eccentricity and critical edge displacement. The fundamental periods were 1.109 s for Model 1 and 0.599 s, 0.672 s, and 0.755 s for Models 2, 3, and 4, respectively. At Mode 15, Models 1-4 achieved cumulative UX/UY participation of 92.88%/95.76%, 93.49%/95.26%, 93.26%/95.69%, and 93.19%/95.50%, respectively, satisfying the 90% criterion in both principal directions. The 0.50 m model is therefore the best-performing tested variant for the adopted global elastic-response metrics, not a universally optimal EBF design.

(2) At the uppermost comparable main-story level, Model 2 reduced Joint 25 displacement from 86.33 mm to 22.91 mm in the Y direction and from 65.27 mm to 28.73 mm in the X direction. The final signed +/-5% accidental-eccentricity drift screening indicates substantial improvement. At the evaluated Joint 25 line, the three braced variants remained below the adopted drift limit; full code compliance nevertheless requires verification of all prescribed edge lines and governing load combinations.

(3) The source storywise torsional ratios decreased in both directions, but torsional irregularity was not eliminated at every story. Model 2 should therefore be described as mitigating torsional severity rather than rendering the building fully regular. Applicable SNI amplification, analysis, and detailing provisions remain in force for the remaining irregularities.

(4) Brace installation substantially redistributed member demands. Selected braced-bay beams experienced large shear increases, selected columns exhibited axial-envelope sign changes, and member torsion generally

decreased in the sampled braced elements. These are demand trends and do not demonstrate RC link, connection, adjacent-member, or foundation capacity.

(5) The study does not establish nonlinear RC link behavior, steel-to-RC connection adequacy, soil-structure or foundation response, economic feasibility, or construction readiness. Code-based member and connection design, support-reaction and foundation checks, nonlinear static and dynamic analyses, and cyclic tests of representative hybrid assemblies are required before application.

ACKNOWLEDGEMENTS

The authors gratefully acknowledge the Department of Civil Engineering, Universitas Brawijaya, for providing computational resources and technical guidance. The authors also thank the anonymous reviewer for comments that improved the definition of the hybrid structural system, the reproducibility of the numerical model, and the limitations of the conclusions.

AUTHOR DECLARATION

Authors' Contributions and Responsibilities. R.M. Simatupang: conceptualization, methodology, validation, formal analysis, writing-original draft, and supervision. C.R.S. Candraningtyas: preliminary design, data curation, software modeling, investigation, and writing-review and editing. Both authors reviewed and approved the manuscript.

Funding. This research received no external funding.

Availability of Data and Materials. Numerical data, ETABS Ultimate v22.0.0 model files, and the available analysis logs are available from the corresponding author upon reasonable request, subject to journal data-sharing requirements.

Competing Interests. The authors declare no competing interests.

REFERENCES

[1] T. Niknam, H. Saberi, V. Saberi, A. Sadeghi, and E. N. Farsangi, "Effect of link beam length of the eccentric bracing system on seismic rehabilitation of weak reinforced concrete frames," Civil and Environmental Engineering Reports, vol. 32, no. 1, pp. 152-175, 2022.

[2] N. Ahmad and M. Masoudi, "Eccentric steel brace retrofit for seismic upgrading of deficient reinforced concrete frames," Bulletin of Earthquake Engineering, vol. 18, no. 6, pp. 2807-2841, 2020.

[3] M. Shayanfar, "Seismic performance of eccentrically braced frames with vertical link using PBPD method," The Structural Design of Tall and Special Buildings, vol. 23, no. 1, pp. 16-32, 2014.

[4] F. Wang, "Cyclic behaviour of Y-shaped eccentrically braced frames fabricated with high-strength steel composite," Journal of Constructional Steel Research, vol. 120, pp. 176-187, 2016.

[5] D. Muhammad, A. Handayani, S. Nastiti, M. Sulthon, P. Susanto, and A. Maulidani, “Comparative study of performance between horizontal and vertical link eccentric braced frames under earthquake load,” IOP Conference Series: Earth and Environmental Science, vol. 1453, Art. no. 012011, 2025.

[6] A. K. Chopra, Dynamics of Structures: Theory and Applications to Earthquake Engineering, 4th ed. Upper Saddle River, NJ, USA: Prentice Hall, 2012.

[7] American Society of Civil Engineers, Minimum Design Loads and Associated Criteria for Buildings and Other Structures, ASCE/SEI 7-16. Reston, VA, USA: ASCE, 2016.

[8] American Institute of Steel Construction, Seismic Provisions for Structural Steel Buildings, ANSI/AISC 341-16. Chicago, IL, USA: AISC, 2016.

[9] Badan Standardisasi Nasional, SNI 1726:2019, Tata Cara Perencanaan Ketahanan Gempa untuk Struktur Bangunan Gedung dan Nongedung. Jakarta, Indonesia: BSN, 2019.

[10] Badan Standardisasi Nasional, SNI 2847:2019, Persyaratan Beton Struktural untuk Bangunan Gedung dan Penjelasan. Jakarta, Indonesia: BSN, 2019.

[11] Badan Standardisasi Nasional, SNI 1727:2020, Beban Desain Minimum dan Kriteria Terkait untuk Bangunan Gedung dan Struktur Lain. Jakarta, Indonesia: BSN, 2020.

[12] Badan Standardisasi Nasional, SNI 1729:2020, Spesifikasi untuk Bangunan Gedung Baja Struktural. Jakarta, Indonesia: BSN, 2020.

[13] Badan Standardisasi Nasional, SNI 7860:2020, Ketentuan Seismik untuk Bangunan Gedung Baja Struktural. Jakarta, Indonesia: BSN, 2020.

[14] Yurisman, B. Budiono, M. Moestopo, and M. Suarjana, “Numerical study on shear link performance in eccentrically braced steel frames,” Jurnal Teknik Sipil, vol. 17, no. 1, pp. 25-38, 2010.

[15] J. W. M. Rafael and A. Y. Lukas, “Comparison study of bracing configuration with shear link in eccentrically braced steel structures,” Journal Innovation of Civil Engineering, vol. 1, no. 1, pp. 7-15, 2020.

[16] Computers and Structures, Inc., ETABS Ultimate, Version 22.0.0, Build 3628, Integrated Building Design Software. Berkeley, CA, USA: CSI.